A Quantitative Study of the Environmental Effects on the Optical Response of Gold Nanorods

Yevgeniy R. Davletshin,[†] Anna Lombardi,[‡] M. Fernanda Cardinal,[§,⊥] Vincent Juvé,[‡] Aurélien Crut,[‡] Paolo Maioli,[‡] Luis M. Liz-Marzán,[⊥] Fabrice Vallée,[‡] Natalia Del Fatti,[‡] and J. Carl Kumaradas*[,†]

[†]Department of Physics, Ryerson University, Toronto, Ontario, M5B 2K3, Canada, [‡]Université Lyon 1, CNRS, LASIM, Villeurbanne Cedex, 69622, France, [§]International Iberian Nanotechnology Laboratory, Braga, 4710229, Portugal, and [⊥]Departamento de Química Física, Universidad de Vigo, Vigo, 36310, Spain

ABSTRACT

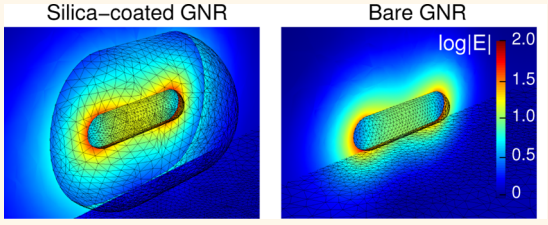

The effects of the dielectric environment on the optical extinction spectra of gold nanorods were quantitatively studied using individual bare and silica-coated nanorods. The dispersion and amplitude of their extinction cross-section, dominated by absorption for the investigated sizes, were measured using spatial modulation spectroscopy (SMS). The experimental results were compared to calculations from a numerical model that included environmental features present in the measurements and the morphology and size of the corresponding nanorods measured by transmission electron microscopy. The combination of these experimental and theoretical tools permits a detailed interpretation of the optical properties of the individual nanorods. The measured optical extinction spectra and the extinction cross-section amplitudes were well reproduced by the numerical model for silica-coated gold nanorods, for which the silica shell provides a controlled environment. In contrast, additional environmental factors had to be assumed in the model for bare nanorods, stressing the importance of controlling and characterizing the experimental conditions when measuring the optical response of bare surface-deposited single metal nanoparticles.

KEYWORDS: gold nanorods · surface plasmon resonance · local fields · environment · spatial modulation spectroscopy · finite element method · silica coating

Over the past decade a large effort has been devoted to studying the size, shape, and environment-dependent optical properties of metal nanoparticles associated with their surface plasmon resonances (SPR). The latter is a consequence of the resonant response of the nanoparticle electrons to the incident electromagnetic field at a specific wavelength and of the concomitant enhancement of the local field experienced by the nanoparticle and its close environment. Owing to their chemical stability, biocompatibility, and SPR in the visible to near-infrared range, gold nanoparticles have been extensively investigated for use in photothermal therapy,[1] photoacoustic imaging,[2] biosensing,[3] surface-enhanced Raman scattering (SERS),[4] and other photonic applications.[5−7] The need to adjust the optical response to specific applications, for example, improving biosensor sensitivity or enhancing the local field effect for SERS applications, has fostered synthesis of nanoparticles of increasingly complex morphology such as nanorods, nanoshells, nanopyramids, nanocages, and nanostars.

Although a good degree of control in synthesis has been reached, the high sensitivity of the optical response of such nanoparticles to their morphology makes it difficult to interpret the optical response measured on ensembles of nanoparticles and to compare the results to theoretical models. Such comparisons can be only done by investigating *individual* nanoparticles of known morphology and developing complete theoretical models that take detailed morphology and experimental conditions into account. This has been done by combining individual nanoparticle spectroscopy with transmission or scanning electron microscopy (TEM or SEM)[8,9] and theoretical models. Such experimental and theoretical combinations can also be used to obtain some information on the morphology and intrinsic characteristics of individual nanoparticles and their environment.[10−15]

For small nanospheres (<20 nm diameter) the SPR wavelength, λ_R, is predominantly determined by the particle's environment, while the SPR extinction cross-section, $\sigma_{ext}(\lambda_R)$, depends on both the particle size and the environment's refractive index.[16,17] Therefore single particle spectroscopy alone can be used to obtain information on the particle's environment, morphology, and intrinsic characteristics, *in situ*.[13] A quasi-static

* Address correspondence to ckumarad@ryerson.ca.

Received for review June 27, 2012 and accepted August 14, 2012.

Published online August 15, 2012
10.1021/nn302869v

approximation based on Mie theory has been predominantly used in this case,[10,13,18] assuming a homogeneous surrounding with an effective index of refraction to represent the effect of the substrate (if present) and other heterogeneities in the particle's environment.[8,19]

For more complex morphologies, such as nanorods, the dependence of the relationship between the optical spectral features and the characteristics of a particle and its environment cannot be disentangled, making it difficult to fully characterize the particle geometry from optical measurements alone. Nanorods exhibit a dominant SPR known as the longitudinal SPR for light polarized along the major axis of the nanoparticle. It shows up as a strong and well-defined band in their extinction and scattering spectra,[14,20] centered at a wavelength that is sensitive to small modifications in their local environment.[21,22] As compared to spheres, the characteristics of the resonance depend also on the shape and aspect-ratio of the particle. If the particle's dielectric function and the environment's refractive index are known, then optical spectroscopy combined with inverse modeling can be used to infer the morphology of the nanoparticle (aspect-ratio and volume).[14,19] Conversely, if the shape and size of the particle are known (using correlated imaging of the particle's morphology), then modeling can provide the refractive index of the environment or the metal's dielectric function, as discussed below. The most common theoretical models have been based on Mie-Gans theory (assuming spheroidal geometry for the particle), but also on numerical methods such as the discrete-dipole approximation (DDA), the boundary element method (BEM), the finite difference time domain (FDTD), and the finite element method (FEM; for arbitrary shaped objects). The FEM allows for easy inclusion of arbitrary heterogeneities such as substrates and particle surface coatings while avoiding dense matrices and will be used here.

Although most investigations have been performed by dispersing the nanoparticles onto a transparent substrate, optical modeling has frequently assumed a homogeneous environment and used an effective refractive index, n_{sur}, as a parameter to describe it.[14,23] The optical response of chemically synthesized nanospheres deposited on a substrate has been observed to largely vary from particle to particle even within the same sample.[12,19] Single particle measurements on elongated nanoparticles have also shown these fluctuations.[24] The presence of embedding polymer matrix has been shown to reduce the sensitivity of the optical properties of gold nanospheres and nanoprisms to the surrounding medium's refractive index.[14,25] These findings raise the important question of the impact of the local environment (*i.e.,* the substrate, surfactant molecules or residual solvent) on the measured optical properties of complex shaped nanoparticles.

We investigated the sensitivity of bare versus silica-coated gold nanorods (GNRs) to their local environment and predicted the effects of a range of hypothetical environmental conditions on the SPR of bare and silica-coated GNRs. This was done by measuring extinction spectra of three bare and three silica-coated GNRs using spatial modulation spectroscopy (SMS), which permits measurement of the extinction cross-section $\sigma_{ext}(\lambda)$, of individual nanoparticles.[13−15] As compared to other single nanoparticle spectroscopy techniques SMS has the key advantage of yielding access not only to the spectrum of the particle optical response but also to its amplitude, that is, to the absolute value of the $\sigma_{ext}(\lambda)$ spectrum, permitting full comparison of experimental and theoretical results. Furthermore, as it is sensitive to both absorption and scattering, smaller particles can be investigated compared to the commonly used scattering based techniques since scattering becoming negligible compared to absorption for small sizes (the size detection limit for gold nanospheres is about 5 nm for SMS as compared to 20 nm for usual dark field spectroscopy). The measured spectra were compared to theoretical spectra using the morphologies and dimensions obtained from TEM and assuming that the particles were on top of a substrate in air. The theoretical modeling was performed by solving the Maxwell's equations with the proper boundary conditions (in particular, taking into account the presence of the substrate) using FEM simulations which used the TEM measured nanoparticle size and shape, and included the size-corrected dielectric function for gold. Finally, a detailed theoretical quantitative analysis was performed on the role of environment on the spectral features.

RESULTS AND DISCUSSION

The extinction spectra of three silica-coated (S-GNR$_1$, S-GNR$_2$, and S-GNR$_3$) and three uncoated GNRs (GNR$_4$, GNR$_5$ and GNR$_6$), spin-coated onto a TEM grid covered by a 40 nm thick silica support substrate (Figure 1a), were measured using SMS (Figure 1b,c). The individual nanorods were detected by demodulating the power of the transmitted light at twice the modulation frequency of the nanoparticle position (see Methods, Optical Characterization). A single particle then shows up as a main peak surrounded by two satellites in the direction of the spatial modulation (Figure 1c). For the investigated GNR sizes, absorption dominates over scattering so that the extinction cross-sections are almost identical to the absorption ones. TEM images of the same six nanorods were recorded (Figure 1d). The dimensions estimated from the TEM images are given in Table 1. The uncertainty in the TEM dimension measurements was approximately ±0.5 nm.

On the basis of these TEM images, a detailed geometric model was created to represent the gold-silica boundary and outer silica surface of the GNR by

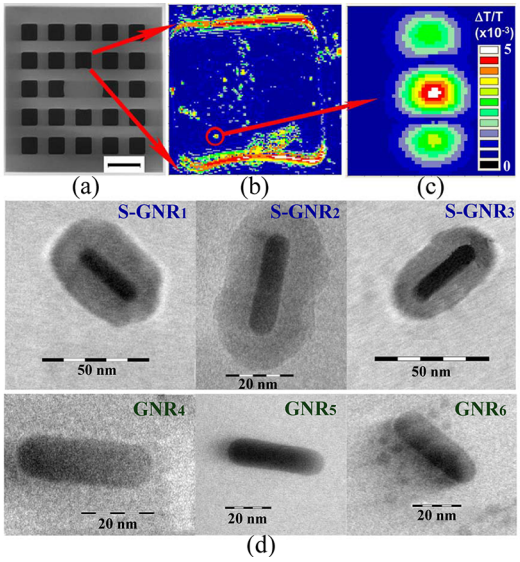

Figure 1. (a) TEM grid showing the 50 μm × 50 μm windows (a silica substrate layer was on top of the windows). The scale bar is 100 μm. (b) Optical SMS image at 800 nm wavelength of one of the grid windows showing different objects. (c) Optical SMS magnified view (1.5 μm × 1.5 μm view) of a gold nanorod. The color-bar in panel c corresponds to the fractional light transmission change due to extinction by the imaged particle (for both panels b and c). (d) TEM images of the six investigated uncoated and silica-coated gold nanorods.

TABLE 1. Dimensions of the Silica-Coated and Bare GNRs Used in the Models[a]

rod	l_e/l_o (nm)	w_e/w_o (nm)	a_e/a_o	s_{tip} (nm)	s_{mid} (nm)
S-GNR$_1$	33.0/33.4	8.8/8.8	3.8/3.8	9.5	15.7
S-GNR$_2$	33.9/34.0	9.3/9.0	3.6/3.8	11.3	15.8
S-GNR$_3$	32.4/31.8	8.8/8.2	3.7/3.9	8.2	9.5
GNR$_4$	38.0/—	11.5/—	3.3/—		
GNR$_5$	40.5/—	10.8/—	3.8/—		
GNR$_6$	39.0/—	12.0/—	3.3/—		

[a] l_e, w_e and a_e are the length, width, and aspect ratio of the nanorods deduced from TEM imaging, respectively. l_o, w_o, and a_o are the refined dimensions deduced from fitting the theoretical model to the optical extinction spectra. s_{tip} and s_{mid} are the silica shell thickness on the tip and on the side of the GNR, respectively (see Figure 2b). It was not possible to deduce refined optical dimensions for the bare GNRs.

using cylinders capped with hemispheres, as shown in Figure 2. To allow for nonuniform silica coating thickness around each GNR, the lengths of the cylindrical section of the gold part and of the cylindrical section of the silica coating were *not* assumed to be identical. The FEM model was used to simulate the extinction spectra of these GNRs under the experimental conditions. Figure 3 provides an example of the surface mesh discretization of the GNR, and substrate, and the amplitude of the total electric field profile around the GNR (of the incident plane wave and of the field scattered by the GNR).

The TEM grid had a thin silica support film. The effect of this film was modeled by a silica substrate layer (n_{sub} = 1.46) as shown in Figure 2. The surroundings were assumed to be air (n = 1.00). The computed optical response of the silica-coated GNRs was very close to the measured optical extinction spectrum (Figure 4a). Due to the large sensitivity of λ_R to the aspect ratio, a refined fitting of the experimental data was performed by slightly resizing the rod length/width (by less than 0.5 nm) and consequently its aspect ratio (Table 1). This refinement fell within the precision of the TEM and optical measurements. The good reproduction of the SPR spectral position and shape for these silica coated nanoparticles validates the use of the dielectric function for gold reported by Johnson & Christy[26] for $\tilde{\varepsilon}_B$ in eq 1, (compared to the Johnson and Christy dielectric data, an approximately 4 nm red or blue shift of λ_R is obtained when using the gold dielectric functions reported by Blanchard[27] or Palik,[28] respectively, for $\tilde{\varepsilon}_B$ in eq 1[14,23]).

The numerical model was unable to reproduce the measured spectra for the bare GNRs using dimensions that were within the TEM measurement uncertainty. The spectra of the bare gold nanorods were then computed using the smallest and largest aspect ratios within the uncertainty limits from the TEM measured dimensions. These spectra strongly deviated from the experimental ones, especially with respect to λ_R, as shown in Figure 4b. Even when using the largest aspect ratio within the uncertainty limits of the TEM measurements, the computed λ_R was blue-shifted by 55−80 nm. Assuming that this discrepancy is due to under-estimation of the rod aspect ratio in the TEM measurements, fitting of the experimental spectra using the rod dimensions as parameters requires an increase of the aspect ratio between 25% and 50% (depending on the GNR), which is incompatible with the precision of the TEM measurements.

For nonspherical particles, such as nanorods, both the object shape and the environment determine λ_R, and a proper reproduction of the measured spectra requires more realistic modeling of the actual environment. Although previous studies have shown that GNRs have octagonal cross-section,[29,30] in the numerical model the GNRs were assumed to have circular cross-sections for simplicity. The level of agreement between the model and the measurement for silica-coated GNRs indicates that this approximation plays a minor role in the modeling. Additionally, surfactant molecules or solvent left during spin-coating of the colloidal solution or a water layer due to humidity may have influenced the measured optical spectra. To provide an insight into the impact of variations in the environment on the extinction spectra of bare and silica-coated GNRs, calculations were performed for different environments for a GNR with gold dimensions corresponding to those of S-GNR$_1$ (Table 1) and the results are shown in Figure 5. As expected, the computed λ_R of the bare GNR shows a large dependence on its surrounding, red-shifting by about 130 nm when changing from a homogeneous air environment

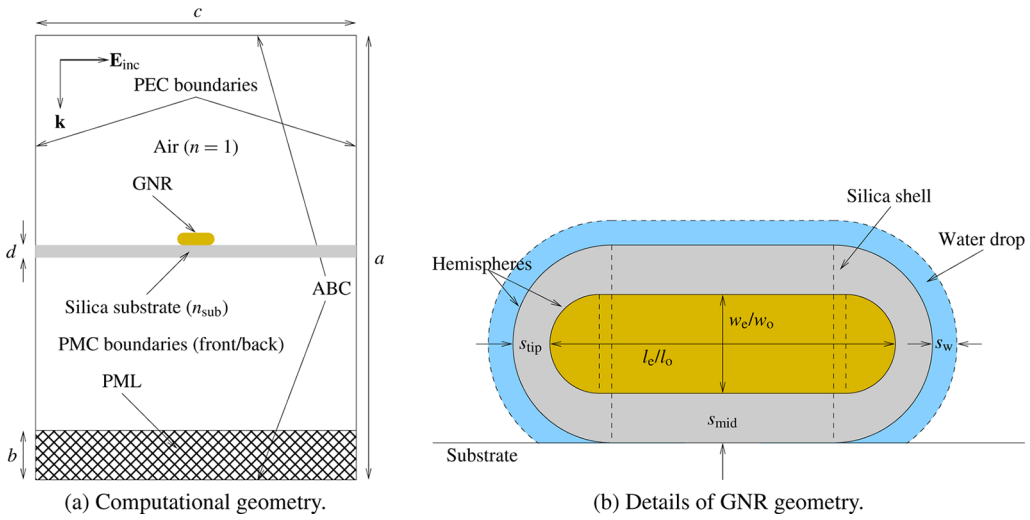

Figure 2. Schematics of the model geometry (not shown to scale). (a) 2D cross-section representation of the 3D geometry and boundary conditions of the computational model. The dimensions were truncated at the top and bottom using an absorbing boundary condition (ABC), at the left and right with a perfect electric conductor (PEC) surface, and at the front and back with a perfect magnetic conductor (PMC) surface. The incident wave was polarized in the left−right direction, traveling downward. Therefore an additional absorbing layer, known as a perfectly matched layer (PML) was placed at the bottom of the domain. The medium inside the domain was air, and the GNR support layer on the TEM grid was modeled as a 40 nm thick silica substrate. In the computational model a = 2400 nm, b = 400 nm, c = 1400 nm, and d = 40 nm. The domain in the front-to-back direction had a size equal to c. (b) Morphology of a GNR used in the model, which assumed cylindrical shape with hemispherical end-tips for both the gold part and the outer silica surface. The various parameters used to define its size are also shown.

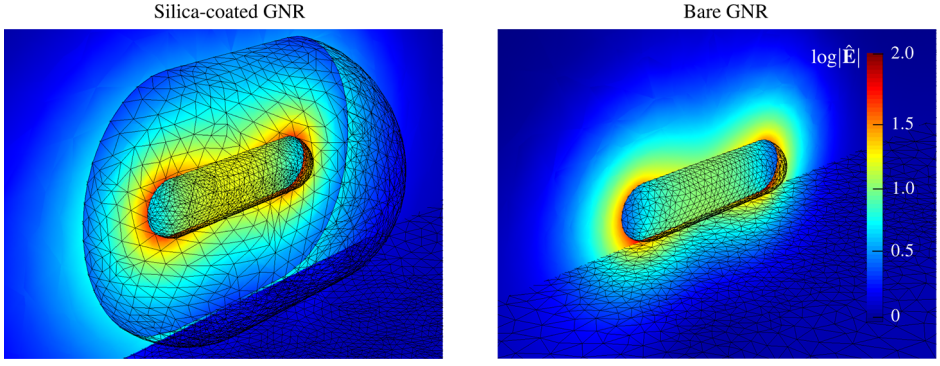

Figure 3. Plots of the *relative* electric field, $\hat{E} = |E|/|E_{inc}|$, where $|E| = (E \cdot E^*)^{1/2}$ is the amplitude of the total electric field and E_{inc} is the amplitude of the incident field. Superimposed on this is the surface discretization of the gold, silica coating, and substrate regions. $\hat{E}$ is shown on a color *log-scale*. Therefore red represents a field amplification of 100×, cyan represents an amplification of 10×, and dark blue represents a field amplitude equal to the incident field. The GNR shown was approximately 33 nm long.

(n_{sur} = 1.00) to a homogeneous water environment (n_{sur} = 1.33). The same nanorod deposited on a silica substrate in air shows an intermediate λ_R, demonstrating that in this inhomogeneous configuration (containing both silica and air) the effective refractive index of a homogeneous surrounding medium is lower than that for water. Conversely λ_R, of the silica-coated GNR exhibits a much smaller environment dependence, only red-shifting by about 20 nm from a homogeneous air to a homogeneous water environment. This reduced sensitivity simply reflects the fact that the plasmonic response of a nanoparticle is sensitive to its environment on the spatial range over which field enhancement takes place, typically of the order of the rod diameter for the investigated rods (Figures 3 and 6a) and of the order of the particle radius for a sphere.[14] Finally, placing a 20 nm water layer around the bare GNR while on the substrate, in air, results in λ_R red-shifting by approximately 100 nm (compared to a red-shift of 10 nm for the silica-coated rod), yielding a value close to what was measured.

As the SMS technique provides a quantitative measurement of light extinction, further information can be obtained by analyzing the amplitude of the measured extinction spectra, $\sigma_{ext}(\lambda_R)$. There are large variations, of up to 800 nm^2 (22% of the mean), in $\sigma_{ext}(\lambda_R)$ in the SMS measurements between the three bare rods shown in Figure 4b. This may be partly accounted for

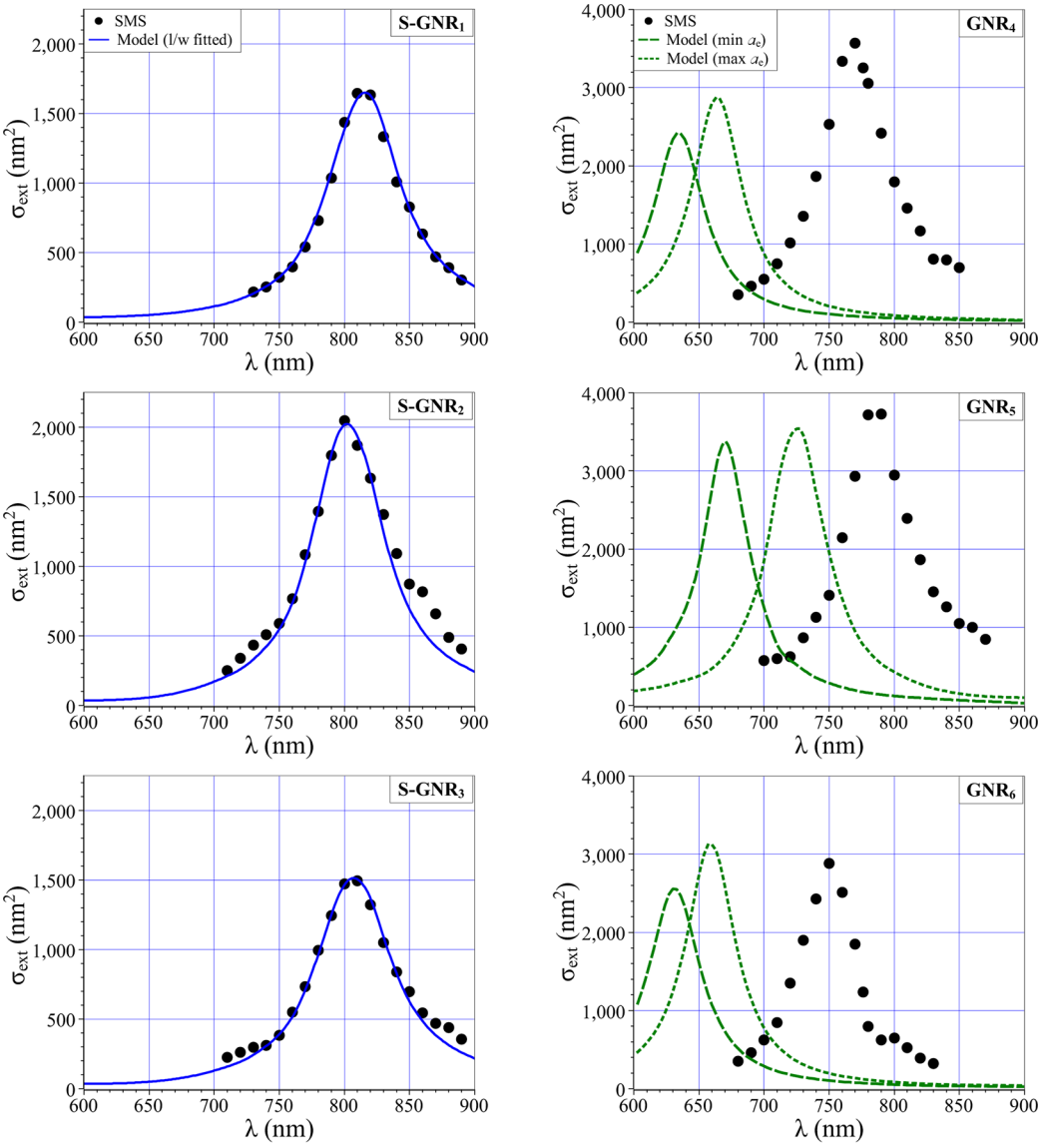

Figure 4. Simulated (solid/dashed/dotted lines) and measured (dots) absolute extinction cross-sections of (a) silica-coated GNR and (b) bare GNRs, all on a silica substrate in air. The simulated spectra shown in the silica-coated GNRs are from a best-fit for the GNR and silica dimensions, as described in the Methods section. The fitted dimensions (Table 1) are within the TEM measurement uncertainty in all three cases. For the bare GNRs, since the GNR aspect ratio affects the extinction peak position, the smallest and largest aspect ratios that fit within the uncertainty of the dimensions from the TEM images (±0.5 nm) were used to produce the two simulated extinction spectra.

by differences in the GNR volumes, but may also be due to environment fluctuations. Figure 5 provides some insight into the effect of the environment on $\sigma_{ext}(\lambda_R)$. The presence of water around the bare GNR (both as an infinite homogeneous medium and as a 20 nm layer on a substrate) increases $\sigma_{ext}(\lambda_R)$ by about 600 nm^2, partly accounting for the observed variations.

A parametric analysis was performed to systematically study the effect of possible contamination on the optical response of bare and coated GNRs. This was done by simulating S-GNR$_1$ with and without its silica shell. In the first study the GNR was surrounded by a drop of water of varying thickness and deposited on a silica substrate layer (see Figure 2b). Figure 6a shows that for silica-coated rods the water droplet on top of the GNR and around its ends produced a weak λ_R red-shift of up to 13 nm, while for bare rods the water layer produced a strong λ_R red-shift up to 100 nm as the drop thickness increases, reaching a plateau after 20 nm in thickness (about 90% of the shift is observed for a thickness of 10 nm, which is of the order of the rod diameter). The effect of the droplet on the spectrum's full-width at half-maximum (fwhm) was also more pronounced for the bare GNR compared to the silica-coated one. This is a consequence of the fact that the decrease in fwhm (for all parametric analyses shown

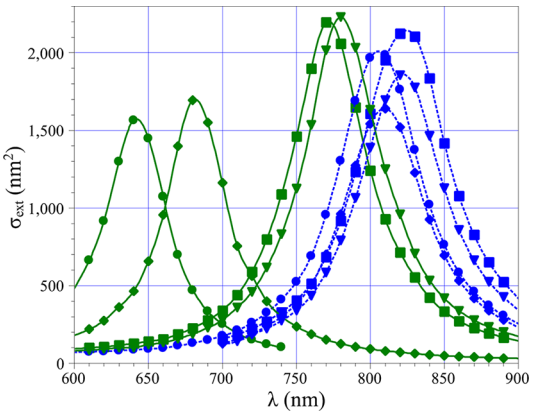

Figure 5. Simulated extinction cross-sections of a silica-coated GNR (blue lines) and a bare GNR (green lines) surrounded by air with no substrate (●), surrounded by water with no substrate (■), deposited on a silica substrate in air (♦), and surrounded by a 20 nm layer of water deposited on a substrate in air (▼; see Figure 2). The gold dimensions are those of S-GNR$_1$ (Table 1).

in Figure 6), given in eV units, is correlated to the shift in λ_R. The decrease in fwhm corresponds to a decrease of the imaginary part of the gold dielectric function as λ_R is shifted away from interband transitions.[10,14,15]

Although the results in Figure 6a are for a hypothetical GNR, its aspect ratio (based on dimensions of the gold part of S-GNR$_1$) is the same as that of GNR$_5$ (see Table 1). The SMS measurements for GNR$_5$ (Figure 4b) produced is λ_R = 785 nm, which was red-shifted from the simulated spectra by between 60 and 115 nm (Figure 4a). Figure 6a shows that a water layer thickness of $s_w \approx 3$ nm on the bare S-GNR$_1$ results in a red-shift of λ_R of $\approx$ 60 nm, and $s_w > 20$ nm results in a red-shift of λ_R of $\approx$ 105 nm. This suggests that a thin layer of water contamination was present during the measurement with a minimum thickness of the order of 3 nm using the water layer geometry shown above (Figure 2). This value has however to be considered as a very rough estimate since the wavelength of the longitudinal SPR of a nanorod is mostly sensitive to the refractive index of its environment around its tips in the rod axis direction, that is, along the substrate plane. Although a nanometer size water layer is expected, the actual thickness experienced by the rod at its tips can thus be larger as the water layer is expected to extend on the substrate plane with a meniscus not accounted for by the model used here (Figure 2). A more realistic geometry for the water layer would include different thickness above the rod and along its main axis direction together with a more realistic water meniscus shape. Furthermore, the ligand molecules bound at the nanoparticle surface may also increase the actual dielectric constant experienced by the rod, an effect not included here.

In contrast to the model used here, the presence of the substrate has been frequently accounted for in many single nanoparticle optical studies assuming that the individual nanoparticles are embedded into an effective homogeneous environment with its refractive index, n_{sur}, used as a fitting parameter.[14,19] Only a few theoretical studies have attempted to include the substrate explicitly in the analysis of single-particle scattering experiments.[31,32] In the homogeneous environment approximation, n_{sur}, thus incorporates the influence of the substrate and other surrounding materials (air, water, or residual solvent and ligand molecules), with a value that is between the substrate's index and the index of the surroundings. Although it constitutes a crude approximation, masking the complexity of the particle environment in the actual single particle geometry, the effective homogeneous environment approximation has been successfully applied to the investigation of single nanospheres (in contrast to GNRs, the dielectric environment and size effects of nanospheres impact independent parameters for the most part, permitting independent and reliable determination of n_{sur} and of the particle size from the SMS optical spectra[14,23]).

In a second parametric study we examined the sensitivity of the spectrum to changes in n_{sur}. As expected, again, the silica-coated rods were much less sensitive to n_{sur} than the bare rods (Figure 6b). λ_R changed by approximately 20 nm for the silica-coated rod compared to a change of approximately 120 nm for the bare rod (similar effects are observed for the fwhm) between air and water. Using this approach (which accounts for the effect of the substrate by using an effective homogeneous environment) one has to use $n_{sur} \approx 1.36$ to reproduce the $\lambda_R \approx 785$ nm measured for GNR$_5$. Although this is in-between the refractive index of air and the silica substrate (n_{sub} = 1.46), it does not mean that a homogeneous surrounding with n_{sub} = 1.36 accounts for only the effect of the substrate. As shown in Figure 4b for GNR$_5$ a model that explicitly included the substrate in air was not able to reproduce the $\lambda_R \approx 785$ nm SMS measurement for GNR$_5$. This indicates that environmental contamination (such as a thin water layer or residual surfactants) must have affected the SMS measurement.

To further analyze the role of the substrate, we have investigated the influence of the substrate refractive index on the SPR characteristics of a silica-coated and a bare GNR. As expected, the silica-coated GNR was less influenced by the substrate than the bare GNR (Figure 6c). λ_R of the silica-coated GNR red-shifted by approximately 5 nm when changing from no substrate (n_{sub} = 1.00) to a high index substrate (n_{sub} = 1.60), whereas it red-shifted by approximately 50 nm for the bare GNR, from no substrate to a high index substrate.

These quantitative investigations of single particle spectroscopy on bare or coated nanoparticles stress the importance of controlling the local nanoparticle environment. The lower sensitivity of silica-coated GNRs directly reflects the fact that nanoparticles experience only their close environment on a distance of

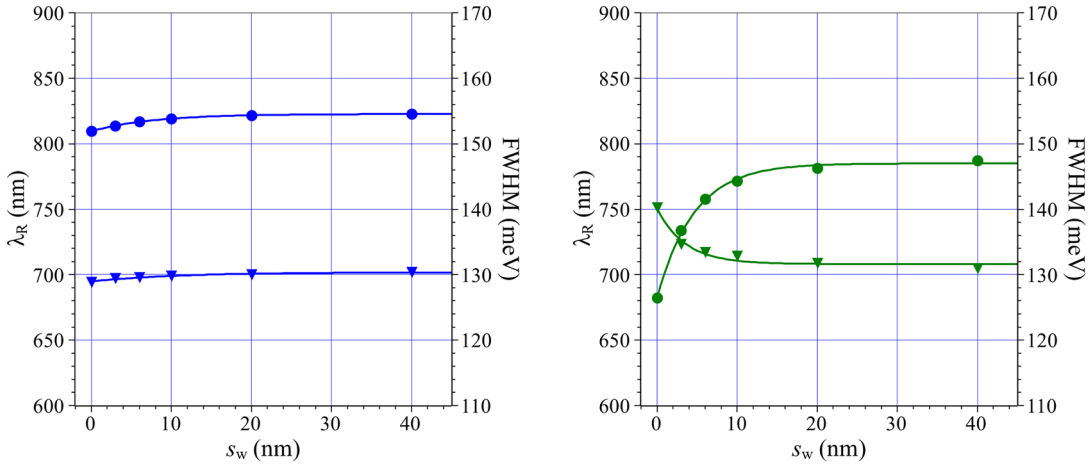

(a) Effect of water droplet size, in air, on a substrate (see Figure 2b)

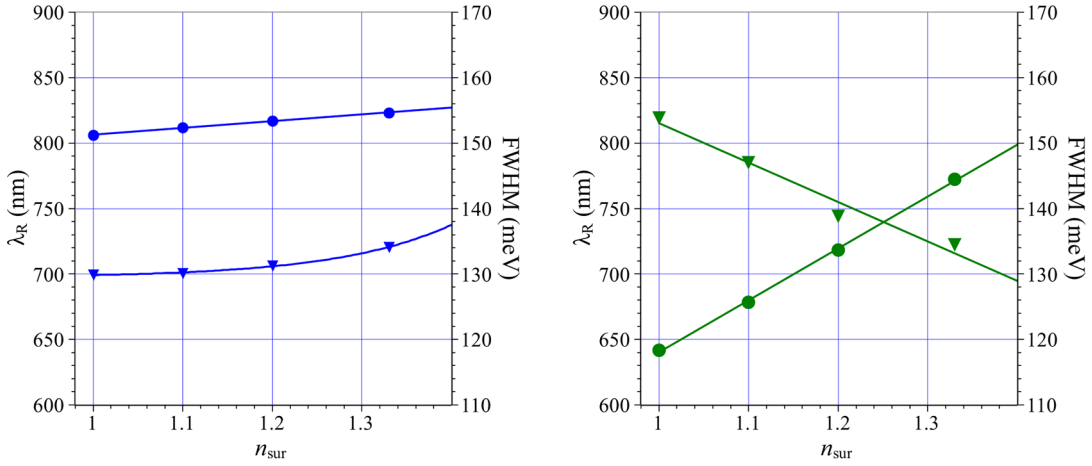

(b) Effect of a homogenous surrounding medium's refractive index, n_{sur}.

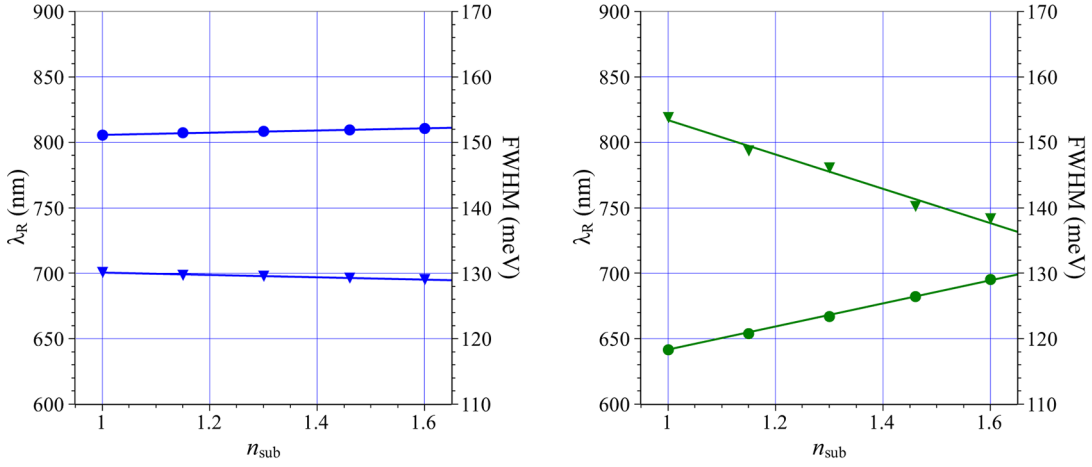

(c) Effect of substrate's refractive index, n_{sub}, in air.

Figure 6. A study of how the surroundings of a silica-coated GNR (left graphs) and a bare GNR (right graphs) affect λ_R (●) and fwhm (▼).

the order of the spatial extent of the local field around the particle at λ_R (Figure 3). This field is of the order of the radius for a sphere,[33,34] or of the width for a GNR (the studied GNRs had widths between approximately 8 and 11 nm).[35] The three GNRs in this study were coated with silica shells of thickness approximately between 8 and 16 nm resulting in the environment having little impact on the GNR's local field.

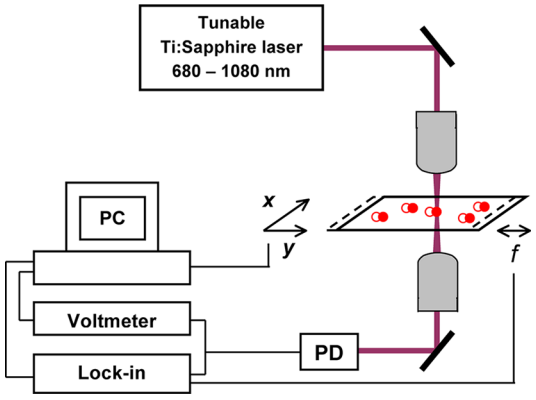

Figure 7. The SMS setup showing the laser source injected into the transmission microscope, which consists of a piezoelectric element modulating the sample position at frequency *f*, the *x*–*y* scanner, the focusing and collecting microscope objective, the Si photodiode (PD), the digital voltmeter, and the lock-in amplifier demodulating the signal.

CONCLUSIONS

The optical extinction spectra of single bare and silica-coated gold nanorods were quantitatively measured around their longitudinal SPR using spatial modulation spectroscopy, and the results were compared to those of a numerical model of optical absorption, taking into account a realistic experimental geometry and the actual nanoparticle morphology and size measured by transmission electron microscopy (extinction is dominated by absorption for the investigated nanorod sizes). The combination of these experimental and theoretical methods constitutes a powerful tool for the detailed interpretation of the optical properties of single nanoparticles. Excellent agreement between the computed and experimental data, that is, surface plasmon resonance wavelength and extinction cross-section amplitude, have been obtained for the silica-coated rods, assuming they are deposited on a silica layer in air using the TEM measured rod dimensions as input. Conversely, a similar analysis with bare rods produced a large deviation of the computed longitudinal SPR wavelengths as compared to the experimental ones due to their large sensitivity to their actual environment. Although a better reproduction of the measurements can be obtained using a mean homogeneous environment approximation, which has been successfully applied to the investigation of single nanospheres, this has been found to mask the actual complexity of the particle environment in single particle measurements. Improved agreement with the optical measurements can also be obtained using a more realistic model assuming that the single nanoparticles deposited on the substrate are embedded within a thin water drop, the latter mimicking the impact of residual solvent, surfactant molecules, or humidity.

These results stress the difficulty in properly describing the measured optical response of a metal nanoparticle deposited onto a substrate, a geometry that is often used in single nanoparticle studies. This problem can be partly solved embedding the particle into a dielectric layer (*e.g.*, polymer film[14]) or dielectric shell to insulate them from uncontrolled environmental conditions. The effects of contamination by a water layer could be avoided by performing single particle spectroscopic measurements in a vacuum chamber. The influence of the local environment on the measured optical properties of single nanoparticles and of the particle to particle variation is similar to that encountered in the investigation of the damping of the acoustic vibration of nanoparticles.[36] This stresses the importance of controlling the local particle environment in single nanoparticle studies, which is efficiently done with silica-coated particles, particularly when the particles have complex shapes.

METHODS

Bare and silica-coated gold nanorods (GNRs) were chemically synthesized as colloidal solutions in an aqueous solvent and spin coated onto a transmission electron microscopy (TEM) grid. The extinction cross-section spectra of individual GNRs on the TEM grid were measured using spatial modulation spectroscopy followed by TEM imaging of the same GNRs. Finite element analysis was used to determine a size, shape, and environment needed to match the observed optical extinction spectrum.

GNR Synthesis. Gold nanorods were synthesized by the seed-mediated growth method in the presence of the cetyltrimethylammonium bromide (CTAB) surfactant.[37] These nanorods are referred to here as bare GNRs. Silica-coated gold nanorods (S-GNR) were prepared by functionalization of CTAB-capped gold nanorods with a thiol-modified poly(ethylene glycol) prior to TEOS condensation.[38] The mean rod aspect ratio, $a = l/w$, was around 3.5, with a mean width, w, of about 10 nm and a silica shell thickness, s, ranging from approximately 8 to 16 nm for the coated rods. After proper dilution, a drop of the solution was spin coated onto a 50 μm × 50 μm window TEM grid covered by a 40 nm thick silica film. The latter provides the required substrate for depositing isolated nanoparticles while permitting both optical and electron transmission measurements. Surface deposited individual GNRs separated by more than 1 μm were obtained, permitting easy optical separation (Figure 1b).

Optical Characterization. Spatial modulation spectroscopy (SMS)[14,19] was used to measure the extinction cross-section of individual GNRs (Figure 7). It is based on the modulation of a particle's spatial position at frequency f, in the focal spot of a tightly focused laser beam. The presence of a nanoparticle induces a modulation of the transmitted light power, with an amplitude proportional to its extinction cross-section $\sigma_{ext}(\lambda)$. The value of the extinction cross-section $\sigma_{ext}(\lambda)$ of a single nanoparticle can thus be measured for sizes down to 5 nm in the case of gold spheres.[14] The $\sigma_{ext}(\lambda)$ spectrum was measured by tuning the wavelength of the light source. For the investigated rods, their longitudinal SPR, that is, for light polarized along their long axis, showed-up around 800 nm. Spectra were thus measured using a Ti:sapphire laser tunable in the 680 to 1080 nm spectral range. The laser beam was focused close to the diffraction limit using a 100× microscope objective with a

numerical aperture of 0.75, yielding a focal spot size of about 0.7λ (full-width at half-maximum of the light intensity profile). The incident mean power was about 10 μW. The sample position was modulated at f = 1.5 kHz. The transmitted light power was collected after the sample by a second microscope objective identical to the focusing one, and detected by a photodiode. Demodulation of the transmitted light amplitude was performed at $2f$ (by a lock-in amplifier) as it permits more precise localization of the particle.[14] The spatial dependence of the signal is approximately proportional to the second derivative in the modulation direction of the beam intensity profile at the focal spot and directly proportional to the beam profile in the direction perpendicular to the modulation direction.[19] When scanning for the location of a particle, a single nanoparticle shows-up as a main peak surrounded by two satellites of opposite sign along the modulation direction (in Figure 1c all the extrema are positive since the absolute value of the transmission change is shown). Measurements of linearly polarized spectra were conducted by rotating the light polarization using a quarter-wave plate and a polarizer.

The optical study was performed prior to the TEM measurements to avoid any influence of substrate or nanoparticle modification by the electron beam. The optical measurements were carried out by detecting the nanoparticle with an SMS optical image with unpolarized light at 800 nm (which is near the longitudinal SPR wavelength of the synthesized nanorods). After locating light responding objects, the sensitivity of the signal amplitude to light polarization was checked to confirm its possible assignment as a single nanorod (for a single GNR there is a very large contrast in the extinction for two orthogonal directions of light polarization around the SPR).[13,39] Its spectrum around the longitudinal SPR was then measured for light polarization along the long axis of the nanoparticle (*i.e.*, the direction maximizing the signal amplitude). The spatial coordinates of its location were thus determined for the follow-up TEM characterization of its geometry and dimensions. TEM images of the six rods are shown in Figure 1d.

Finite Element Model. A finite element model was built using a commercially available finite element software, COMSOL Multiphysics (COMSOL Inc., Burlington, MA), taking into account the dimensions of GNRs from TEM measurements and a realistic geometry of the SMS setup that included the TEM grid silica substrate (Figure 2). The incident electric field, $\mathbf{E}_{inc}$, propagated in the downward direction (relative to Figure 2) with a polarization in the left/right direction (along the longitudinal axis of the nanorod).

Although the experiment consisted of an unbounded domain, the computational model had to be artificially truncated using appropriate boundary conditions in all directions (see Figure 2a). Ideally boundary conditions such as an absorbing boundary condition (ABC) and/or a perfectly matched layer (PML) would be used to minimize the effect of the artificial boundaries. Initial testing using combined ABC/PML boundaries to truncate computational domain produced good results in the simulations of the electromagnetic wave propagation in a homogeneous environment, but led to artifacts in simulations where the substrate was adjacent to the boundary. Perfect electrical conductor (PEC) boundaries, $\mathbf{n} \times \mathbf{E} = 0$, and perfect magnetic conductor (PMC) boundaries, $\mathbf{n} \times \mathbf{H} = 0$, which simulate periodic structures when the boundaries are perpendicular to the incident electric and magnetic fields, respectively, were used in place of absorbing boundaries. The PEC/PMC boundaries were placed sufficiently far from the GNR such that the distance between the periodic GNR structures were large enough to prevent coupling between them. The PEC and PMC boundary conditions were used at the boundaries perpendicular and parallel to the incident electric field polarization, respectively. The top and the bottom boundaries of the model had an ABC imposed on them using a Sommerfeld radiation condition.[40] The ABC was used so that the boundary appears transparent to the incident radiation and absorbs the scattered field. All internal boundaries had tangential E-field continuity (ensured by the use of vector basis functions[41]). The dimensions of the computational domain were chosen so that any further increase in the domain size did not alter the solution. This ensured that all the artificial external boundaries did not introduce artifacts into the model.

The refractive index of the nanorod's silica shell and the TEM silica substrate were set to a constant value of n = 1.46.[42] As usually done for metal nanoparticles, the dielectric function of the gold part, $\tilde{\varepsilon}_{GNR}$, was obtained from the bulk one, $\tilde{\varepsilon}_B$,[26] and corrected for intrinsic size effects. For the sizes investigated here, the intrinsic properties related to GNR size were included by modifying the electron scattering rate γ_D of the conduction electrons in the Drude term of the gold dielectric function to take into account additional electron scattering off the nanoparticle's surface.[33] For confined electrons it can be written as

$$\tilde{\varepsilon}_{GNR} = \tilde{\varepsilon}_B + \frac{\omega_p^2}{\omega^2 + i\omega\gamma_{D_0}} - \frac{\omega_p^2}{\omega^2 + i\omega\left(\gamma_{D_0} + \frac{Av_F}{L_{eff}}\right)} \quad (1)$$

where γ_{D_0} is the bulk like electron scattering rate in the particle and v_F is the electron Fermi velocity. A is a dimensionless parameter representing details of the electron interactions with the confining surface, and L_{eff} is an effective mean free path of the surface confined electrons. L_{eff} corresponds to the particle diameter for spherical nanoparticles,[33,43,44] while for nonspherical objects its appropriate dimension dependence remains an ongoing area of investigation. A simple billiard type model produced the relationship, $L_{eff} = 4V/S$, where V is the volume and S is the surface area of the object.[45] Note that L_{eff} varies weakly for the investigated particles. A different dependence on their dimensions only leads to different A values when reproducing the measured spectra.

The surface confinement broadening parameter was assumed to have a constant value of A = 0.5. This reproduced the longitudinal SPR fwhm of the three silica-coated GNRs to within 1% and the fwhm of the simulated bare rods were 5% to 10% lower than the measured fwhm. Since this value was used for nanorods of very similar sizes, the dependency of the fwhm on the mean free path of the conduction electrons, L_{eff}, was not tested. In addition, the imaginary part of the bulk gold dielectric function[26] has been suspected of being inaccurate in the spectral range used in the experiments,[15] complicating the quantitative estimation of A from measured spectra. Though the assumed A value is consistent with a previous investigation,[46] a more reliable determination requires investigation of the fwhm as a function of the nanorod dimensions[46] in a controlled environment, which would reduce chemical damping effects due to surface bound molecules, as was recently done for nanospheres.[43]

Meshing was performed with tetrahedral elements used with quadrilateral vector basis functions.[41] The resulting mesh had approximately 370 000 to 540 000 elements, resulting in approximately 2−4 million degrees of freedom. After computation of the electromagnetic field, the absorption cross-section σ_{abs} of a nanorod was obtained by integrating the absorbed power density over the volume V of its gold part divided by the incident light intensity:

$$\sigma_{abs}(\omega) = \frac{2}{c\varepsilon_0|\mathbf{E}_{inc}|^2}\int_V \mathcal{R}\{\sigma(\omega)\mathbf{E}\cdot\mathbf{E}^* - i\omega\mathbf{E}\cdot\mathbf{D}^*\}\,dV \quad (2)$$

where $\mathbf{E}$ and $\mathbf{D}$ are the electric and displacement field at the frequency ω, respectively, and $\sigma = \omega\mathcal{I}\{\tilde{\varepsilon}_{GNR}\}$ is the conductivity of the gold nanorod. The $\mathcal{R}\{\}$ and $\mathcal{I}\{\}$ operators produce the real and imaginary components of the complex integrand, respectively. The scattering cross-section σ_{sca} was calculated from the outgoing electromagnetic energy flux over a surface S surrounding the gold nanorod:

$$\sigma_{sca}(\omega) = \frac{2}{c\varepsilon_0|\mathbf{E}_{inc}|^2}\oint_S \mathcal{R}\{\mathbf{E}_{sca} \times \mathbf{H}_{sca}^*\}\,dS \quad (3)$$

where $\mathbf{E}_{sca}$ and $\mathbf{H}_{sca}$ are the scattered electric and magnetic fields at the frequency ω, respectively.

The extinction cross-section σ_{ext} was then obtained as the sum of absorption and scattering: $\sigma_{ext} = \sigma_{abs} + \sigma_{sca}$. For the small-size bare or silica-coated nanorods investigated here, absorption dominates over scattering (simulations showed that $\sigma_{sca}(\lambda_R)/\sigma_{abs}(\lambda_R) < 0.01$) so that $\sigma_{ext} = \sigma_{abs}$ was assumed.

The effect of light reflected by the TEM grid substrate during the SMS measurements of σ_{ext} was removed by a normalizing against a transmission measurement through a section of the substrate where no GNRs were present. Since the computational model calculated σ_{abs} which was assumed to be equal to σ_{ext}, incident light reflected by the silica substrate had no effect on the theoretical σ_{ext} calculation.

Conflict of Interest: The authors declare no competing financial interest.

Acknowledgment. The authors acknowledge support from the Canadian Natural Sciences and Engineering Research Council (Discovery Grant No. 312235-06), Ministère des Affaires étrangères et européennes Project PICASSO 22930NE, and the Spanish MINECO (Project No. MAT2010-15374). N.D.F. acknowledges support from Institut Universitaire de France (IUF). M.F.C. acknowledges a Ph.D. fellowship from INL.

REFERENCES AND NOTES

1. Huang, X.; Jain, P. K.; El-Sayed, I. H.; El-Sayed, M. A. Plasmonic Photothermal Therapy (PPTT) Using Gold Nanoparticles. *Lasers Med. Sci.* **2008**, *23*, 217–228.
2. Yang, X.; Stein, E.; Ashkenazi, S.; Wang, L. Nanoparticles for Photoacoustic Imaging. *WIREs Nanomed. Nanobiotechnol.* **2009**, *1*, 360–368.
3. Mayer, K. M.; Hafner, J. H. Localized Surface Plasmon Resonance Sensors. *Chem. Rev.* **2011**, *111*, 3828–3857.
4. Huang, X.; El-Sayed, I. H.; Qian, W.; El-Sayed, M. A. Cancer Cells Assemble and Align Gold Nanorods Conjugated to Antibodies to Produce Highly Enhanced, Sharp, and Polarized Surface Raman Spectra: A Potential Cancer Diagnostic Marker. *Nano Lett.* **2007**, *7*, 1591–1597.
5. Jain, P. K.; Huang, X.; El-Sayed, I. H.; El-Sayed, M. A. Noble Metals on the Nanoscale: Optical and Photothermal Properties and Some Applications in Imaging, Sensing, Biology, and Medicine. *Acc. Chem. Res.* **2008**, *41*, 1578–1586.
6. Sau, T. K.; Rogach, A. L.; Jäckel, F.; Klar, T. A.; Feldmann, J. Properties and Applications of Colloidal Nonspherical Noble Metal Nanoparticles. *Adv. Mater.* **2010**, *22*, 1805–1825.
7. Garcia, M. A. Surface Plasmons in Metallic Nanoparticles: Fundamentals and Applications. *J. Phys. D: Appl. Phys.* **2011**, *44*, 283001.
8. Billaud, P.; Marhaba, S.; Cottancin, E.; Arnaud, L.; Bachelier, G.; Bonnet, C.; Del Fatti, N.; Lermé, J.; Vallée, F.; Vialle, J.-L.; *et al*. Correlation between the Extinction Spectrum of a Single Metal Nanoparticle and Its Electron Microscopy Image. *J. Phys. Chem. C* **2008**, *112*, 978–982.
9. Cottancin, E.; Celep, G.; Lermé, J.; Pellarin, M.; Huntzinger, J.; Vialle, J.; Broyer, M. Optical Properties of Noble Metal Clusters as a Function of the Size: Comparison between Experiments and a Semi-quantal Theory. *Theor. Chem. Acc.* **2006**, *116*, 514–523.
10. Sönnichsen, C.; Franzl, T.; Wilk, T.; von Plessen, G.; Feldmann, J. Drastic Reduction of Plasmon Damping in Gold Nanorods. *Phys. Rev. Lett.* **2002**, *88*, 1–4.
11. Novo, C.; Gomez, D.; Perez-Juste, J.; Zhang, Z.; Petrova, H.; Reismann, M.; Mulvaney, P.; Hartland, G. V. Contributions from Radiation Damping and Surface Scattering to the Linewidth of the Longitudinal Plasmon Band of Gold Nanorods: A Single Particle Study. *Phys. Chem. Chem. Phys.* **2006**, *8*, 3540–3546.
12. Berciaud, S.; Cognet, L.; Tamarat, P.; Lounis, B. Observation of Intrinsic Size Effects in the Optical Response of Individual Gold Nanoparticles. *Nano Lett.* **2005**, *5*, 515–518.
13. Muskens, O.; Christofilos, D.; Del Fatti, N.; Vallée, F. Optical Response of a Single Noble Metal Nanoparticle. *J. Opt. A: Pure Appl. Opt.* **2006**, *8*, S264–S272.
14. Muskens, O. L.; Bachelier, G.; Del Fatti, N.; Vallée, F.; Brioude, A.; Jiang, X.; Pileni, M.-P. Quantitative Absorption Spectroscopy of a Single Gold Nanorod. *J. Phys. Chem. C* **2008**, *112*, 8917–8921.
15. Baida, H.; Christofilos, D.; Maioli, P.; Crut, A.; Del Fatti, N.; Vallée, F. Surface Plasmon Resonance Spectroscopy of Single Surfactant-Stabilized Gold Nanoparticles. *Eur. Phys. J. D* **2011**, *63*, 293–299.
16. Genzel, L.; Martin, T. P.; Kreibig, U. Dielectric Function and Plasma Resonances of Small Metal Particles. *Z. Phys. B* **1975**, *21*, 339–346.
17. Kraus, W.; Schatz, G. Plasmon Resonance Broadening in Small Metal Particles. *J. Chem. Phys.* **1983**, *79*, 6130–6139.
18. Sancho-Parramon, J. Surface Plasmon Resonance Broadening of Metallic Particles in the Quasi-Static Approximation: A Numerical Study of Size Confinement and Interparticle Interaction Effects. *Nanotechnology* **2009**, *20*.
19. Muskens, O.; Billaud, P.; Broyer, M.; Del Fatti, N.; Vallée, F. Optical Extinction Spectrum of a Single Metal Nanoparticle: Quantitative Characterization of a Particle and of its Local Environment. *Phys. Rev. B* **2008**, *78*, 1–9.
20. Hartland, G. V. Optical Studies of Dynamics in Noble Metal Nanostructures. *Chem. Rev.* **2011**, *111*, 3858–3887.
21. Becker, J.; Trügler, A.; Jakab, A.; Hohenester, U.; Sönnichsen, C. The Optimal Aspect Ratio of Gold Nanorods for Plasmonic Bio-Sensing. *Plasmonics* **2010**, *5*, 161–167.
22. Otte, M. A.; Sepúlveda, B.; Ni, W.; Juste, J. P.; Liz-Marzán, L. M.; Lechuga, L. M. Identification of the Optimal Spectral Region for Plasmonic and Nanoplasmonic Sensing. *ACS Nano* **2010**, *4*, 349–357.
23. Billaud, P.; Huntzinger, J.-R.; Cottancin, E.; Lermé, J.; Pellarin, M.; Arnaud, L.; Broyer, M.; Del Fatti, N.; Vallée, F. Optical Extinction Spectroscopy of Single Silver Nanoparticles. *Eur. Phys. J. D* **2007**, *43*, 271–274.
24. Lombardi, A.; Loumaigne, M.; Crut, A.; Maioli, P.; Del Fatti, N.; Vallée, F.; Spuch-Calvar, M.; Burgin, J.; Majimel, J.; Tréguer-Delapierre, M. Surface Plasmon Resonance Properties of Single Elongated Nano-Objects: Gold Nanobipyramids and Nanorods. *Langmuir* **2012**, *28*, 9027–9033.
25. Novo, C.; Funston, A. M.; Pastoriza-Santos, I.; Liz-Marzan, L. M.; Mulvaney, P. Influence of the Medium Refractive Index on the Optical Properties of Single Gold Triangular Prisms on a Substrate. *J. Phys. Chem. C* **2008**, *112*, 3–7.
26. Johnson, P.; Christy, R. Optical Constants of the Noble Metals. *Phys. Rev. B* **1972**, *6*, 4370–4379.
27. Blanchard, N. P.; Smith, C.; Martin, D. S.; Hayton, D. J.; Jenkins, T. E.; Weightman, P. High-Resolution Measurements of the Bulk Dielectric Constants of Single Crystal Gold with Application to Reflection Anisotropy Spectroscopy. *Phys. Stat. Sol. (c)* **2003**, *0*, 2931–2937.
28. Palik, D. E. *Handbook of Optical Constants of Solids*; Academic Press: Orlando, FL, 1985; p 804.
29. Wang, Z.; Mohamed, M.; Link, S.; El-Sayed, M. Crystallographic Facets and Shapes of Gold Nanorods of Different Aspect Ratios. *Surf. Sci.* **1999**, *440*, L809–L814.
30. Carbó-Argibay, E.; Rodríguez-González, B.; Gómez-Graña, S.; Guerrero-Martínez, A.; Pastoriza-Santos, I.; Pérez-Juste, J.; Liz-Marzán, L. M. The Crystalline Structure of Gold Nanorods Revisited: Evidence for Higher-Index Lateral Facets. *Angew. Chem.* **2010**, *122*, 9587–9590.
31. Vernon, K. C.; Funston, A. M.; Novo, C.; Gómez, D. E.; Mulvaney, P.; Davis, T. J. Influence of Particle-Substrate Interaction on Localized Plasmon Resonances. *Nano Lett.* **2010**, *10*, 2080–2086.
32. Knight, M. W.; Wu, Y.; Lassiter, J. B.; Nordlander, P.; Halas, N. J. Substrates Matter: Influence of an Adjacent Dielectric on an Individual Plasmonic Nanoparticle. *Nano Lett.* **2009**, *9*, 2188–2192.
33. Kreibig, U.; Vollmer, M. *Optical Properties of Metal Clusters*; Springer Series in Materials Science; Springer: New York, 1995.
34. Evanoff, D. D.; White, R. L.; Chumanov, G. Measuring the Distance Dependence of the Local Electromagnetic Field from Silver Nanoparticles. *J. Phys. Chem. B* **2004**, *108*, 1522–1524.
35. Liz-Marzán, L. M.; Pérez-Juste, J.; Pastoriza-Santos, I. Plasmonics of Gold Nanorods. Considerations for Biosensing. *NATO Secur. Sci.* **2008**, 103–111.
36. Voisin, C.; Christofilos, D.; Del Fatti, N.; Vallée, F. Environment Effect on the Acoustic Vibration of Metal Nanoparticles. *Phys. B* **2002**, *316-317*, 89–94.

37. Nikoobakht, B.; El-Sayed, M. A. Preparation and Growth Mechanism of Gold Nanorods (NRs) Using Seed-Mediated Growth Method. *Chem. Mater.* **2003**, *15*, 1957–1962.
38. Fernández-López, C.; Mateo-Mateo, C.; Alvarez-Puebla, R. A.; Pérez-Juste, J.; Pastoriza-Santos, I.; Liz-Marzán, L. M. Highly Controlled Silica Coating of PEG-Capped Metal Nanoparticles and Preparation of SERS-Encoded Particles. *Langmuir* **2009**, *25*, 13894–13899.
39. Baida, H.; Christofilos, D.; Maioli, P.; Crut, A.; Del Fatti, N.; Vallée, F. Surface Plasmon Resonance Linear and Nonlinear Response in a Single Nanorod. *Proc. SPIE* **2008**, *7033*, 703319.
40. Sommerfeld, A. *Partial Differential Equations in Physics*; Academic Press Inc.: New York, 1949.
41. Jin, J.-M. *The Finite Element Method in Electromagnetics*, 2nd ed.; John Wiley & Sons: New York, 2002.
42. Mutilin, S. V.; Khasanov, T. The Refractive Index of Homogeneous SiO_2 Thin Films. *Opt. Spectrosc.* **2008**, *105*, 461–465.
43. Baida, H.; Billaud, P.; Marhaba, S.; Christofilos, D.; Cottancin, E.; Crut, A.; Lermé, J.; Maioli, P.; Pellarin, M.; Broyer, M.; *et al.* Quantitative Determination of the Size Dependence of Surface Plasmon Resonance Damping in Single Ag@SiO_2 Nanoparticles. *Nano Lett.* **2009**, *9*, 3463–3469.
44. Lermé, J.; Baida, H.; Bonnet, C.; Broyer, M.; Cottancin, E.; Crut, A.; Maioli, P.; Del Fatti, N.; Vallée, F.; Pellarin, M. Size Dependence of the Surface Plasmon Resonance Damping in Metal Nanospheres. *J. Phys. Chem. Lett.* **2010**, *1*, 2922–2928.
45. Coronado, E. A.; Schatz, G. C. Surface Plasmon Broadening for Arbitrary Shape Nanoparticles: A Geometrical Probability Approach. *J. Chem. Phys.* **2003**, *119*, 3926–3934.
46. Carey, C. R.; LeBel, T.; Crisostomo, D.; Giblin, J.; Kuno, M.; Hartland, G. V. Imaging and Absolute Extinction Cross-Section Measurements of Nanorods and Nanowires through Polarization Modulation Microscopy. *J. Phys. Chem. C* **2010**, *114*, 16029–16036.